

SciDVS: A Scientific Event Camera with 1.7% Temporal Contrast Sensitivity at 0.7 lux

Rui Graca, Sheng Zhou, Brian McReynolds, Tobi Delbruck
Sensors Group, Inst. of Neuroinformatics, UZH-ETH Zurich, Zurich, Switzerland
 rpgraca,shengzhou,bmac,tobi@ini.uzh.ch, <https://sensors.ini.ch>

Abstract—This paper reports a Dynamic Vision Sensor (DVS) event camera that is 6x more sensitive at 14x lower illumination than existing commercial and prototype cameras. Event cameras output a sparse stream of brightness change events. Their high dynamic range (HDR), quick response, and high temporal resolution provide key advantages for scientific applications that involve low lighting conditions and sparse visual events. However, current DVS are hindered by low sensitivity, resulting from shot noise and pixel-to-pixel mismatch. Commercial DVS have a minimum brightness change threshold of $>10\%$. Sensitive prototypes achieved as low as 1%, but required kilo-lux illumination. Our SciDVS prototype fabricated in a 180nm CMOS image sensor process achieves 1.7% sensitivity at chip illumination of 0.7lx and 18 Hz bandwidth. Novel features of SciDVS are (1) an auto-centering in-pixel preamplifier providing intrascene HDR and increased sensitivity, (2) improved control of bandwidth to limit shot noise, and (3) optional pixel binning, allowing the user to trade spatial resolution for sensitivity.

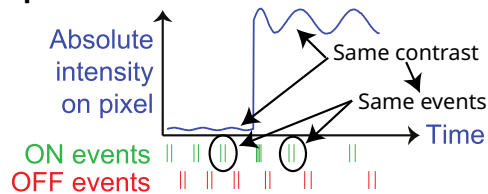
I. INTRODUCTION

Fig. 1A illustrates how a Dynamic Vision Sensor (DVS) pixel encodes brightness changes into sparse, activity-driven events [1]–[13]. Its logarithmic response provides High Dynamic Range (HDR). The low-latency and sparse events enable high-speed vision with low computational complexity.

Sensing small temporal contrast with an event camera would benefit applications such as fluorescent imaging of neural activity and space domain awareness. These applications require a sensitivity of $<10\%$ and are characterized by sparse periods of rapid activity, require HDR, and must operate with dim lighting. They currently rely on high speed sCMOS cameras with limited Dynamic Range (DR) and highly redundant frame output. Recent commercial DVS development focuses on reducing pixel size [9]–[13], which impacts sensitivity by increasing shot noise and pixel-to-pixel mismatch [14]. Previous sensitive DVS cameras achieved higher sensitivity in bright settings [4]–[6] by adding a preamplifier between photoreceptor and change amplifier. The increased gain allows smaller Nominal Contrast Threshold (NCT) without having too many “hot” pixels (induced by event threshold mismatch) that have extremely high noise event rates.

However, no prior DVS camera has demonstrated sub-10% sensitivity under dim illumination conditions, mainly because noise in DVS pixels was not understood. Sensitive DVS designs required very bright illumination (on the order of klx). Bright illumination is not available for neural imaging, where the fluorescence signal emitted by the tissue is a minuscule fraction of the incident light; or for space applications, where

A: DVS pixel function



B: SciDVS requirements and solutions

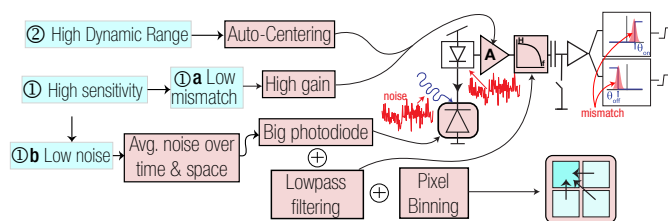


Fig. 1. A: Principle of DVS operation with varying HDR illumination [2]. B: Scientific DVS requirements and SciDVS solutions.

stars and satellites are dim points against a dark background. Under dark conditions, shot noise is the dominant factor limiting sensitivity [14], [15]. The SciDVS camera reported in this paper exploits the recent understanding [16] that DVS photoreceptor noise can reach a minimum of 2x photon shot noise by properly biasing the photoreceptor and its buffer.

Photon shot noise introduces a fundamental limit to the visual process. As shown by Rose [15], for a single pixel to reliably detect an edge with contrast C , it needs to accumulate a number of photons proportional to $1/C^2$. Since the minimum contrast detectable by a DVS defines its sensitivity, when operating at the 2x shot noise limit, increasing sensitivity is equivalent to accumulating more photons. This can be done spatially, by increasing the photodiode area, or temporally, by low-pass filtering the photoreceptor output.

Fig. 1B illustrates how SciDVS addresses the requirements for a scientific event camera by combining several solutions: ① High-sensitivity demands: ①a low pixel-to-pixel mismatch, which is met by introducing a preamp as in [4]–[6], and ①b low noise, which is met by combining larger spatial integration using a large photodiode, as well as a novel binning technique, and longer temporal integration using an optimized low-pass filter. ② The HDR requirement is met by a novel auto-centering circuit for the preamp.

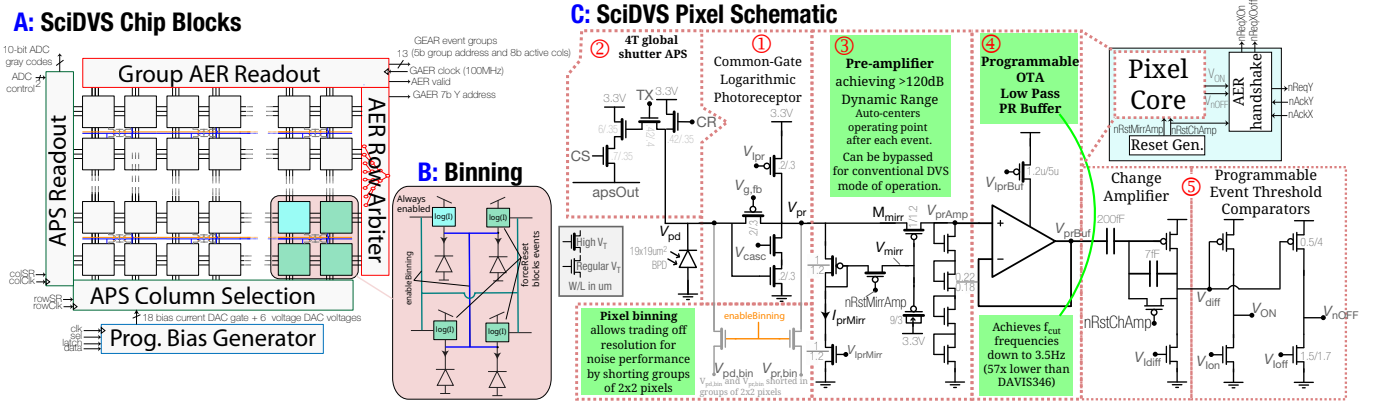


Fig. 2. Circuits. **A:** Chip block diagram with APS readout [3], group AER readout [9], and bias generators [17] **B:** 2×2 binning that shorts photodiode/photoreceptor outputs and can optionally disable $\frac{3}{4}$ of event generators. **C:** pixel schematic, with novel SciDVS features in green boxes.

II. DESCRIPTION OF KEY FEATURES

Fig. 2A shows the SciDVS block diagram, which includes Group AER readout [9], 9b APS global shutter frames (not concurrent with events) [3], and programmable biases [17].

Fig. 2B&C shows the novel SciDVS binning mode. Binning is widely used for low-light CIS. A pixel binning concept for foveated DVS proposed photocurrent summing [18]. SciDVS shorts both photodiodes (V_{pd}) and photoreceptors (V_{pr}) of 2×2 pixel groups. Enabling `enableBinning` reduces $V_{rms}(V_{pr})$ by 2x. Due to mismatch, each pixel has a slightly different threshold, so the outputs are not necessarily redundant. Enabling `forceReset` additionally reduces output event rate by disabling 3 of the 4 event generators in a pixel bin.

Fig. 2C shows the pixel circuits. Photocurrent generated in the buried photodiode can be steered by adjusting the biases and control signals to the DVS common-gate photoreceptor ① or to the 4T APS frame readout ② from [3]. The APS readout is enabled by setting $V_{g,fb} = V_{Vdd}$ which steers photocurrent to the APS readout. The column reset CR, select CS, transfer gate TX, and source-follower output `apsOut` are as in [3]. Setting CR=0 steers current to the DVS photoreceptor.

The photoreceptor output V_{pr} is amplified by the preamp ③ based on the diode-stack from [18]. The preamp mirrors the photocurrent with M_{mirr} and then applies this current to a stack of diode-connected transistors providing a gain of ≈ 7 . The preamp output V_{prAmp} is proportional to the log of the mirrored photocurrent, with a gain dependent only on the thermal voltage and the weak inversion slope of the transistors in the stack, hence subject to low mismatch.

In [4], [6], the increase in gain introduced by preamplification results in a decrease in intrasene DR to only about 60dB centered around the array-level average illumination, thus losing a key DVS advantage. Ref. [5] addressed this problem by adding pixel-level adaptation of the preamp operating point using a pseudo-resistor. It provides standard DVS HDR, but the adaptation time after a high contrast edge is slow, temperature dependent, and mismatch-prone.

The SciDVS preamp overcomes the DR limitation in [4] by introducing a 3T-1C pixel-level auto-centering circuit: After each event, `nRstMirrAmp` is temporarily activated,

establishing a circuit path that sets V_{mirr} to mirror I_{prMirr} , re-centering the dynamic range for that pixel. The preamp can be bypassed (by switches not shown) for standard DVS operation. The preamp output V_{prAmp} drives a 5T OTA low-pass buffer ④, that is designed with long, thick-gate, high V_T FETs to improve the source follower stage by allowing f_{cut} bandwidths 57x smaller than in previous DVS, allowing the user to trade speed for sensitivity. The change detector and threshold comparators ⑤ use the proven topology from previous DVS [2]–[4], [6]–[11].

III. RESULTS AND COMPARISON

Fig. 3 shows the response of the SciDVS array to pulses of various contrast, from which the NCT is inferred. The curves show the fraction of pixels that respond to a step of a given contrast C , obtained by applying a high-contrast ($\approx 60\%$) reset pulse, followed by a test step with contrast C . A pixel is considered to respond to a step if it outputs an event with the correct polarity in a 200ms window following the step. The NCT is defined as the contrast step to which 50% of the pixels respond. Using noisy settings underestimates the NCT due to constructive contribution of noise to the step (stochastic resonance) [19]. Therefore, the measurements were done at 40lx chip illuminance with binning activated to minimize shot-noise (Fig. 5A) and thus make the most accurate estimate of NCT. With the preamp enabled, NCT OFF/ON of 0.84%/1.52% are achievable, with 0% of the pixels responding with events of either polarity in response to a step of 0 contrast (i.e., no step) (see inset). This NCT is $>10x$ smaller than standard DVS mode (preamp bypassed).

Fig. 4 compares DVS sensitivity under low (0.7lx) and extremely low (12 mlx) white LED chip illumination with two commercial DVS cameras. These chip illumination levels correspond to scene illumination at dim indoor (20 lx) and full moon (0.3 lx) conditions [20]. For both illumination conditions and all sensors, we optimized NCT, f_{cut} and refractory period to maximize edge detection, while keeping the noise event rate under 6 Hz/px. The rotating chart has large contrast 20% edges to reset the pixels, and low contrast ON and an OFF test edges from the set of low contrasts 1% to 3.9%. Each image shows events accumulated over a 200 ms window. To quantify

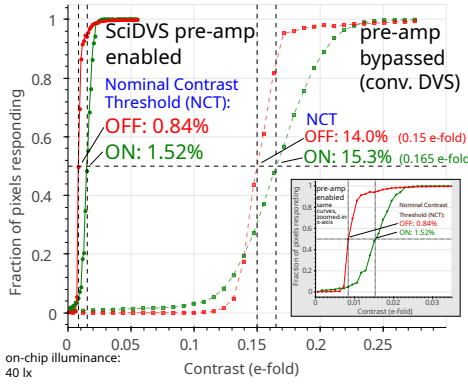


Fig. 3. SciDVS chip NCT sensitivity measurement. Compares SciDVS to preamp-disabled conventional DVS operation.

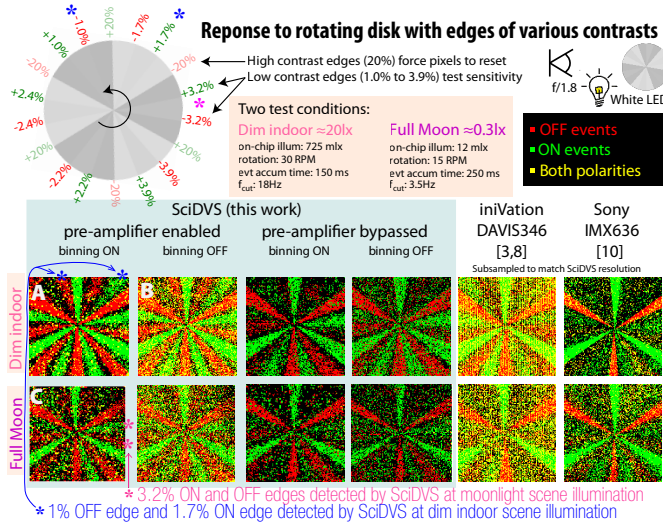


Fig. 4. SciDVS and commercial DVS response to rotating disk with low contrast edges. On-chip illumination measured from calibrated test pixel photoreceptor output voltage. Video: <https://youtu.be/k6CwX8yGOuU>.

sensitivity, an edge is considered detected if at least 50% of the pixels respond with the correct polarity event during the 200 ms accumulation time.

Under dim indoor chart illumination SciDVS reliably detects the OFF edge of 1%, and the ON edge of 1.7% (image **A** blue *). SciDVS clearly outperforms both SciDVS with preamp bypassed and the commercial DVS where these edges are not visible in the images. Turning SciDVS binning off (image **B**) increases edge detection probability through stochastic resonance, but the noise rate is much higher as can be seen from the large number of yellow pixels.

With full moon chart illumination, SciDVS reliably detects the 3.2% edges (image **C** magenta *). These edges are not visible from SciDVS with the preamp disabled or from the commercial DVS.

We can examine the plausibility of these results with Eq. (1), which estimates the per-pixel photoelectrons N transduced during the integration time $\tau \approx 1/(2\pi f_{\text{cut}})$:

$$N[e^-] \approx L[\text{lx}] \times 10^4 \text{ ph/lx/s}/\mu\text{m}^2 \times \text{QE} \times (30 \mu\text{m})^2 \times 4 \times \tau[\text{s}] \quad (1)$$

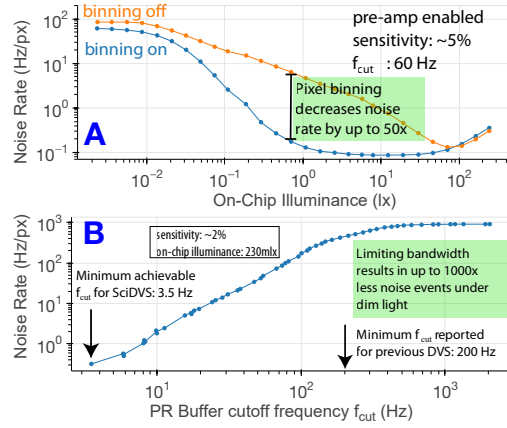


Fig. 5. Measured noise event rates. **A**: vs. illuminance with pixel binning on and off (array level). **B**: vs. PR buffer cutoff frequency f_{cut} (test pixel)

where L is the chip illuminance in lx, the conversion factor of 10^4 from lx to visible photons comes from [15], Quantum Efficiency (QE) $\approx 50\%$, and the factor of 4 accounts for binning. The minimum possible DVS photoreceptor noise predicted by [16] is then $\sigma = \sqrt{2N}$ and $\sigma/N = \sqrt{2/N}$.

For $L=0.7 \text{ lx}$ and $f_{\text{cut}}=18 \text{ Hz}$, $N=110 \text{ ke}^-$ and $\sigma/N = 0.4\%$, and for $L=12 \text{ mlx}$ and $f_{\text{cut}} = 3.5 \text{ Hz}$, $N=10 \text{ ke}^-$ and $\sigma/N = 1.4\%$. The observed sensitivities of 1.7% and 3.2% are respectively 4.2 and 2.2 times the predicted $1\text{-}\sigma$ shot noise and therefore plausible. Moreover, they suggest that SciDVS can be operated near the theoretical 2x shot noise limit.

Fig. 5A plots chip-level average pixel noise rate vs. illuminance with and without binning enabled for very sensitive NCT $\approx 5\%$. Binning reduces noise event rate per pixel in the $1/4$ of active pixels by 50x at medium-low illumination. This noise reduction effect of binning is also visible when comparing the SciDVS images in Fig. 4: The ones with binning are quieter; the background wedges have fewer noise events. Fig. 5B plots noise rate versus f_{cut} with extremely low NCT $\approx 2\%$ and 210 mlx chip illuminance. Reducing f_{cut} to 3.5 Hz reduces the noise event rate to 0.1 Hz/px, a factor of 1000x smaller than at the 200 Hz minimum f_{cut} from the DAVIS346 [16].

Fig. 6 shows several high sensitivity event accumulation frames, a high dynamic range scene, where part of the sensor was covered by an ND4 filter, and a SciDVS APS image. High speed operation is demonstrated by accumulating events for 309 μs to reconstruct the “SLOW” text at an equivalent of $\approx 3 \text{ kHz}$ frame rate.

Table I is a comparison table, labeled die photo, and photo of the prototype camera. SciDVS achieves 6x better sensitivity than commercial DVS at 14x dimmer light [10], and achieves 1.7% sensitivity at 3 500x lower illumination than the previously reported sensitive prototype [5].

ACKNOWLEDGEMENTS:

Funded by Swiss National Science Foundation project SCIDVS (200021_185069). We thank SC Liu for their helpful comments.

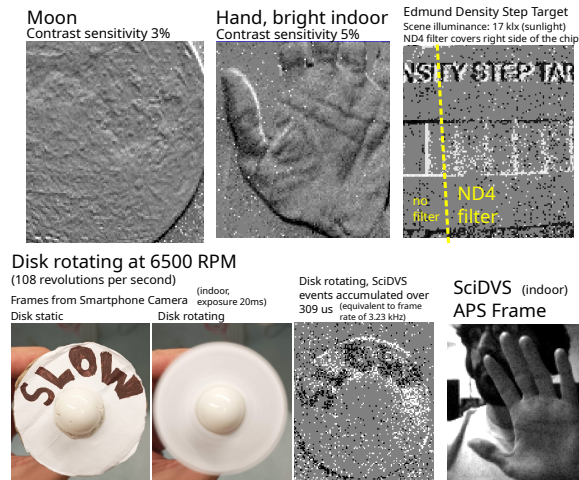


Fig. 6. SciDVS sample recordings. Video: https://youtu.be/I3bse3z_ET0.

TABLE I
COMPARISON TABLE, DIE PHOTO WITH 2X2 PIXEL LAYOUT AND CAMERA.

	This work	JSSC 2013 [4]	JSSC 2015 [3]	inVation DAVIS346 [7,9]	inVation DVXplorer [8]	Sony IMX636 [5]
Tech.	180nm 1P6M FSI	350nm 2P4M FSI	180nm 1P6M FSI	180nm 1P6M FSI	90/40nm 1P5M BSI	90/40nm BSI
Pitch (μm)	30	31	31.2	18.5	9	4.86
Array	126x112	128x128	60x30	346x260	640x480	1280x720
Fill Factor (%)	40	10.5	10.3	22	NA	>77
Power/px (μW)	0.3 ^f	0.24	0.4	0.1	0.088	0.035
Min f_{cut} (Hz)	3.5	NA	NA	200	NA	NA
Min NCT (%) ^a	1.7@0.7x 3.2@1.2x 8.4@3.5x	1.5@NA	1@2.5kx	14.3@NA	9@NA	11@10x
DR (dB) ^b	>120	60	130 ^c	120	80	>124
Max EPS (Hz) ^d	332M	20M	NA	50M	300M	1G
Intensity Frames	Yes ^e	No	No	Yes	No	No

^a Min NCT at specified chip illuminance and f_{cut} . SciDVS from Fig. 4 measurements with binning. ^b Intrascene. ^c with slow adaptation of preamp operating levels. ^d Peak die-level event readout rate; severely limited by interface, e.g. USB. ^e Alternative to events. ^f When biased for low noise.

REFERENCES

- [1] G. Gallego, T. Delbruck, G. M. Orchard, *et al.*, “Event-based vision: A survey,” *IEEE Trans. Pattern Anal. Mach. Intell.*, 2020. DOI: 10.1109/TPAMI.2020.3008413.
- [2] P. Lichtsteiner and T. Delbruck, “A 64x64 AER logarithmic temporal derivative silicon retina,” in *Research in Microelectronics and Electronics, 2005 PhD*, vol. 2, 2005, pp. 202–205. DOI: 10.1109/RME.2005.1542972.
- [3] C. Brandli, R. Berner, M. Yang, S. Liu, and T. Delbruck, “A 240 × 180 130 dB 3 μs latency global shutter spatiotemporal vision sensor,” *IEEE Journal of Solid-State Circuits*, vol. 49, no. 10, pp. 2333–2341, 2014. DOI: 10.1109/JSSC.2014.2342715.
- [4] T. Serrano-Gotarredona and B. Linares-Barranco, “A 128 × 128 1.5% contrast sensitivity 0.9% FPN 3 μs latency 4 mW asynchronous frame-free dynamic vision sensor using transimpedance preamplifiers,” *IEEE Journal of Solid-State Circuits*, vol. 48, no. 3, pp. 827–838, Mar. 2013, ISSN: 1558-173X. DOI: 10.1109/JSSC.2012.2230553.
- [5] M. Yang, S. Liu, and T. Delbruck, “A dynamic vision sensor with 1% temporal contrast sensitivity and in-pixel asynchronous delta modulator for event encoding,” *IEEE Journal of Solid-State Circuits*,

vol. 50, no. 9, pp. 2149–2160, Sep. 2015. DOI: 10.1109/JSSC.2015.2425886.

- [6] D. P. Moeys, F. Corradi, C. Li, *et al.*, “A sensitive dynamic and active pixel vision sensor for color or neural imaging applications,” *IEEE Transactions on Biomedical Circuits and Systems*, vol. 12, no. 1, pp. 123–136, Feb. 2018, ISSN: 1940-9990. DOI: 10.1109/TBCAS.2017.2759783.
- [7] G. Taverni, D. P. Moeys, F. F. Voigt, *et al.*, “In-vivo imaging of neural activity with dynamic vision sensors,” in *2017 IEEE Biomedical Circuits and Systems Conference (BioCAS)*, 2017, pp. 1–4. DOI: 10.1109/BIOCAS.2017.8325076.
- [8] G. Taverni, D. Paul Moeys, C. Li, *et al.*, “Front and back illuminated dynamic and active pixel vision sensors comparison,” *IEEE Transactions on Circuits and Systems II: Express Briefs*, vol. 65, no. 5, pp. 677–681, 2018. DOI: 10.1109/TCSII.2018.2824899.
- [9] B. Son, Y. Suh, S. Kim, *et al.*, “A 640×480 dynamic vision sensor with a 9μm pixel and 300Meps address-event representation,” in *2017 IEEE International Solid-State Circuits Conference (ISSCC)*, Feb. 2017, pp. 66–67. DOI: 10.1109/ISSCC.2017.7870263.
- [10] T. Finatou, A. Niwa, D. Matolin, *et al.*, “A 1280×720 back-illuminated stacked temporal contrast event-based vision sensor with 4.86μm pixels, 1.066GEPS readout, programmable event-rate controller and compressive data-formatting pipeline,” in *2020 IEEE International Solid-State Circuits Conference - (ISSCC)*, 2020, pp. 112–114. DOI: 10.1109/ISSCC19947.2020.9063149.
- [11] M. Guo, S. Chen, Z. Gao, *et al.*, “A 3-wafer-stacked hybrid 15MPixel CIS + 1 MPixel EVS with 4.6GEvent/s readout, in-pixel TDC and on-chip ISP and ESP function,” in *2023 IEEE International Solid-State Circuits Conference (ISSCC)*, 2023, pp. 90–92. DOI: 10.1109/ISSCC42615.2023.10067476.
- [12] A. Niwa, F. Mochizuki, R. Berner, *et al.*, “A 2.97μm-pitch event-based vision sensor with shared pixel front-end circuitry and low-noise readout mode,” in *2023 IEEE International Solid-State Circuits Conference (ISSCC)*, 2023, pp. 4–6. DOI: 10.1109/ISSCC42615.2023.10067566.
- [13] K. Kodama, Y. Sato, Y. Yorikado, *et al.*, “1.22μm 35.6Mpixel RGB hybrid event-based vision sensor with 4.88μm-pitch event pixels and up to 10K event frame rate by adaptive control on event sparsity,” in *2023 IEEE International Solid-State Circuits Conference (ISSCC)*, 2023, pp. 92–94. DOI: 10.1109/ISSCC42615.2023.10067520.
- [14] R. Graça, B. McReynolds, and T. Delbruck, “Shining light on the DVS pixel: A tutorial and discussion about biasing and optimization,” in *2023 IEEE/CVF Conference on Computer Vision and Pattern Recognition Workshops (CVPRW)*, 2023, pp. 4045–4053. DOI: 10.1109/CVPRW59228.2023.00423.
- [15] A. Rose, *Vision: Human and Electronic*. Springer US, 1973. DOI: 10.1007/978-1-4684-2037-1.
- [16] R. Graca, B. McReynolds, and T. Delbruck, “Optimal biasing and physical limits of dvs event noise,” in *2023 International Image Sensor Workshop (IISW)*, 2023. DOI: arXiv:2304.04019.
- [17] M. Yang, S.-C. Liu, C. Li, and T. Delbruck, “Addressable current reference array with 170db dynamic range,” in *2012 IEEE International Symposium on Circuits and Systems (ISCAS)*, 2012, pp. 3110–3113. DOI: 10.1109/ISCAS.2012.6271979.
- [18] T. Serrano-Gotarredona, F. Faramarzi, and B. Linares-Barranco, “Electronically foveated dynamic vision sensor,” in *2022 IEEE International Conference on Omni-layer Intelligent Systems (COINS)*, 2022, pp. 1–5. DOI: 10.1109/COINS54846.2022.9855009.
- [19] B. J. McReynolds, R. Graca, L. Kulesza, and P. McMahon-Crabtree, “Re-interpreting the step-response probability curve to extract fundamental physical parameters of event-based vision sensors,” in *Unconventional Imaging IV*, SPIE Photonics Europe, vol. 12996, SPIE, 2024, p. 1 299 659. DOI: arXiv:2404.07656.
- [20] T. Delbruck, *Notes on practical photometry for image sensor and vision sensor developers*, 1997. DOI: 10.5167/uzh-258967.